Original Article

Longitudinal *in vivo* intrinsic optical imaging of cortical blood perfusion and tissue damage in focal photothrombosis stroke model

Shanshan Yang[1,*], **Kezhou Liu**[2,3,*], **Huijie Ding**[3], **Huan Gao**[4], **Xiaoxiang Zheng**[2,4,5], **Zhihua Ding**[1], **Kedi Xu**[2,4,5,*] **and Peng Li**[1,*]

Abstract

A thorough understanding of the spatiotemporal dynamics of blood supply and tissue viability is of great importance in stroke researches. In the current study, vascular and cellular responses to focal ischemia were monitored with optical coherence tomography on chronic rat photothrombotic stroke model. The 3D mapping of blood perfusion and cellular scattering were achieved by analyzing the temporal dynamics and depth attenuation of intrinsic backscattered light respectively. Optical coherence tomography revealed that vessels of different types presented various spatial and temporal dynamics during the photothrombotic occlusion and the later recovery period. The large distal middle cerebral arteries presented a spontaneous recanalization and the small pial microvessels presented a reperfusion along with newly appeared vessels from the peripheral into the core area. The cortical capillary perfusion presented a weak recovery. Compared to the male group, the female rats showed a faster vascular recovery after photothrombotic. Moreover, the dynamic changes of the cellular scattering signal showed a high spatial and temporal correlation with the cortical capillary perfusion. Combined with well-designed photothrombotic stroke model and chronic optical window, optical coherence tomography imaging offers a unique approach to improve the understanding of stroke procedure and evaluate the treatment outcomes.

Introduction

Focal ischemic stroke is the leading cause of death and disability worldwide.[1,2] The cerebrovascular embolization in stroke deprives blood supply and causes ischemia of surrounding tissue, resulting in cellular damage and neural dysfunction. The current treatments for acute ischemic stroke aim to restore the

[1]State Key Lab of Modern Optical Instrumentation, College of Optical Science and Engineering, Zhejiang University, Hangzhou, Zhejiang, China
[2]Department of Biomedical Engineering, Key Laboratory of Biomedical Engineering of Education Ministry, Zhejiang University, Hangzhou, China
[3]College of Life Information Science and Instruments Engineering, Hangzhou Dianzi University, Hangzhou, China
[4]Qiushi Academy for Advanced Studies (QAAS), Zhejiang University, Hangzhou, China
[5]Zhejiang Provincial Key Laboratory of Cardio-Cerebral Vascular Detection Technology and Medicinal Effectiveness Appraisal, Zhejiang University, Hangzhou, China

*These authors contributed equally to this work.

Corresponding authors:
Peng Li, State Key Lab of Modern Optical Instrumentation, College of Optical Science and Engineering, Zhejiang University, Room 311, #3 Teaching Building, #38 Zheda Road, Hangzhou 310027, China.
Email: peng_li@zju.edu.cn
Kedi Xu, Department of Biomedical Engineering, Key Laboratory of Biomedical Engineering of Education Ministry, Zhejiang University. #2 the Old Biomedical Engineering Building, #38 Zheda Road, Hangzhou, China 310027.
Email: xukd@zju.edu.cn

blood flow to the ischemic region in appropriate time point.[3] Experimental data and clinical evidences show that the outcome of cellular and brain function recovery is highly related to the reperfusion of microvascular circulation, especially in the penumbra area.[4,5] There is a critical need to address the understanding of the mechanisms how the cerebral blood flow adapts and the brain tissue reacts to a focal ischemia insult. More intensively understanding of the recovery process after stroke with or without different interventions will definitely help to improve the long-term outcome of the vast majority of stroke victims. In order to achieve this goal, it is essential to have noninvasive techniques for chronic tracking of the vascular and cellular changes after stroke.

Due to the high spatial and temporal resolution, optical imaging techniques have been widely adopted in the studies of the dynamic changes of vascular structure and blood perfusion with acute and chronic stroke models.[6–11] Two-photon (2P) microscopy is capable of direct visualization of the elaborate vessel organization and measuring the red blood cell (RBC) flux in individual capillaries by tracking exogenous contrast agents, which has a sub-cellular imaging resolution and a imaging depth of several hundred micrometer into the living brain.[7,8] However, 2P microscope normally has a slow scan speed and a limited field-of-view, which is not applicable for the purpose of assessing large scale blood flow in typical stroke models. In addition, when using 2P microscopy with stroke model, the ischemia damage of cortical tissue could induce the leakage of exogenous dye and impede the possible imaging of microvasculature.[9] Thus, stroke studies would in particular benefit from intrinsic contrast blood flow signal without introducing exogenous agents into the bloodstream. Contrary to 2P microscopy, laser speckle contrast imaging (LSCI) is capable of label-free blood flow mapping utilizing dynamic light scattering, and can measure relative changes of cerebral blood flow (CBF) with a larger field-of-view.[10] As an extension to LSCI, multi-exposure speckle imaging (MESI) can provide high quantitative accuracy of CBF dynamics, which assists the characterization of perfusion progression after ischemic stroke.[11] However, both LCSI and MESI remain depth-integrated imaging techniques and are lack of capillary resolution, which cannot provide valuable blood flow information of the deeper cortex layer.

Optical coherence tomography (OCT) is an emerging optical imaging modality, which performs three-dimensional (3D) volumetric imaging of the internal microstructure in biological tissue over 1–2 mm imaging scale with micron-meter resolution.[12] OCT measures the echoes of backscattered light of scatters. The moving red blood cells give rise to dynamic light scattering and can be used as the surrogate of the flowing blood.[13] The 3D mapping of blood perfusion, usually termed as OCT angiography (OCTA), can then be achieved by mathematically analyzing the motion-induced temporal dynamics of optical scattering signals.[13–18] Compared with other real-time optical techniques, OCTA enables an *in vivo* visualization of 3D blood perfusion in the tissue bed down to capillary level.[14,19–21] The intrinsic motion contrast of OCTA eliminates the requirement of contrast dye injection. In addition, the light scattering signal is extremely sensitive to the morphological changes of cells and organelles which are strongly related to the tissue and cellular pathophysiological status.[22–24] Thus, by extracting the scattering coefficient from the depth attenuation of OCT scattering signal, OCT might offer a complementary indicator of brain damage and recovery. Longitudinal OCT imaging has been carried out on the transient filament middle cerebral arteries occlusion (MCAO) stroke model to analyze the spatiotemporal interplay between hemodynamics and cell viability.[25–27] Although the MCAO stroke model has many similar characteristics with clinical stroke patients, this model is limited in the spatial specificity to some extent. OCT has also been reported for studying the vascular remodeling in permanent stroke model with a target artery permanently occluded with microbipolar coagulation. The procedure of electrical coagulation is relatively invasive and is prone to cause mechanical damage to the cortex.[28] To overcome these disadvantages of MCAO and microbipolar coagulation stroke models, photothrombotic (PT) stroke model has gradually been adopted due to its precise space specificity and non-contact characteristics, which allows targeting of any cortical area of interest in a reproducible and less invasive way.[29] Combined with chronic optical window, vessel occlusion can be easily induced by laser irradiation through transparent coverglass over the cortex to mimic focal ischemia damage of the brain.[9] Although the hemodynamics after PT stroke has been studied with 2P and LSCI,[30,31] to our knowledge, no study of chronic hemodynamics changes has been reported using OCT with PT stroke model in rats.

In this work, parallel studies of the spatiotemporal dynamics of blood perfusion and tissue scattering were performed with OCT on the chronic rat PT stroke model. The gender differences of the vascular and cellular responses were investigated. We hypothesized that the functional recovery of the blood vessels and tissue following ischemic stroke was a key role in the therapy methods against brain damage. Our finding revealed the dynamics changes of the blood vessels and tissue after ischemic stroke, suggesting OCT as a promising tool for performance evaluation of the future stroke therapy.
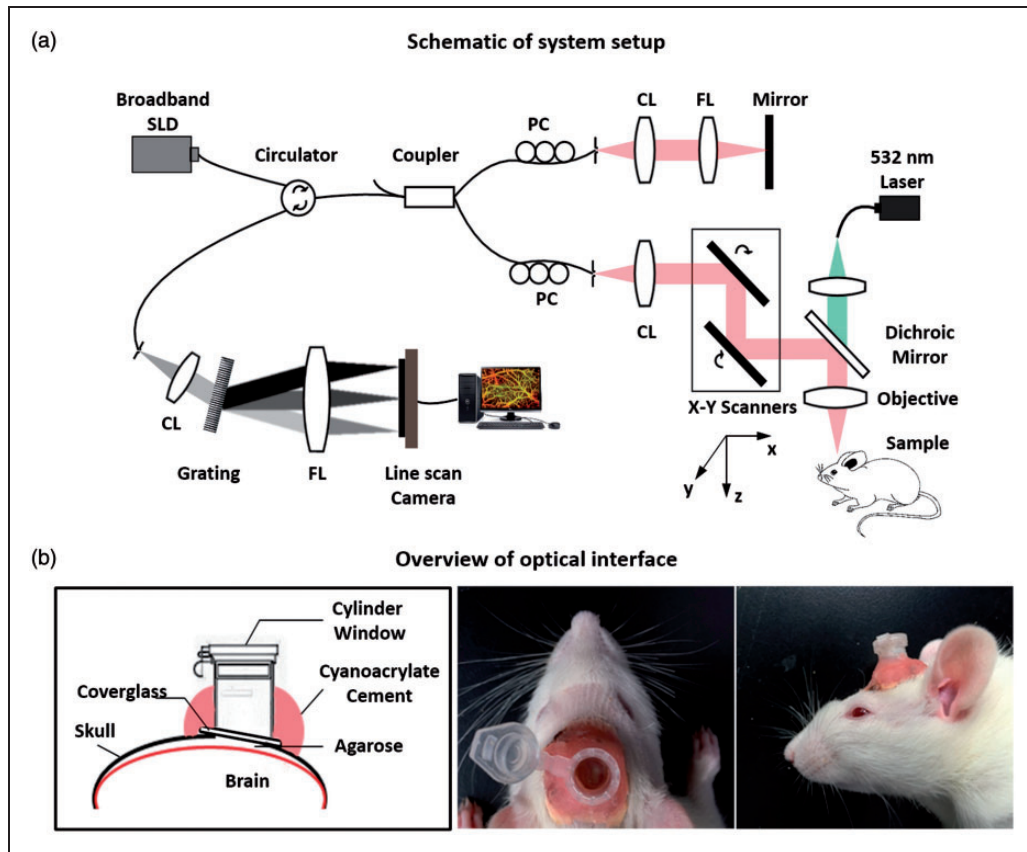
Figure 1. (a) Schematic of the system setup. (b) Overview of the optical window interface on rat for inducing photothrombotic (PT) stroke and OCT imaging.
SLD: superluminesent diode; PC: polarization controller; CL: collimate lens; FL: focus lens; Grating: transmission grating diffraction.

Method

OCTA setup and scanning protocol

The imaging system used in this study was based on a typical configuration of spectral domain OCT as shown in Figure 1(a). A broadband super luminescent diode (Thorlabs, Newton, NJ, USA, SLD1325) was used as the light source. This light source had a central wavelength of 1325 nm and a full width at half maximum bandwidth of 100 nm, theoretically offering a high axial resolution of ~7.6 μm in air at zero light path and 8.5 μm at 2 mm depth. The output light was delivered into a 2×2 fiber coupler and split into the reference and sample arms. In the sample arm, an x–y galvanometer was adopted for 3D volume scanning. An objective lens with focal length of 36 mm was used to focus probing light beam on the region of interest, yielding a lateral resolution about 10 μm and a depth of focus around 122 μm. The OCT detection unit was a high-speed spectrometer equipped with a fast line-scan InGaAs camera, providing a 120 kHz line-scan rate with 2048 active

pixels. The spectrometer had a designed spectral resolution of 0.076 nm, providing an imaging range of ~2.9 mm on each side of the zero delay line in air.

In this study, a stepwise raster scanning protocol was used to acquire volumetric dataset (z–x–y). The slow-scanner (y direction) was driven by a step waveform with a total of 512 steps. At each step, five repeated B-frames were successively acquired for analyzing dynamic flow signals, with each B-frame composed of 512 A-lines in the fast-scan (x) direction. The repeated B-frame scanning was designed to suppress the decorrelation noise in blood flow imaging.[32] Each 3D data set need a total acquisition time of ~13.4 s and covers a 2×2 mm spatial region in x–y plane. Finally, a raw data cube of spectral interferogram $S(k, x, y, t)$ was generated for each 3D volume scan, where k is the wavenumber, and t is the number of the repeated B-frame at each scanning step y. To increase the field of view of cerebral blood perfusion, a montage scanning protocol was implemented to acquire three individual cube scans (field of view: 2×2 mm). The individual cube scans located at different pre-defined

grids with a ~50% overlap between adjacent cubes, allowing enough space to stitch the images together without missing information. After all three-cube scans were collected, post-processing was performed to obtain the vascular images, which were then stitched together to form a large field of view (3.6×1.8 mm^2).

Animal preparation and assemble of long-lasting optical window

All experiments were conducted on adult male and female Sprague–Dawley rats obtained from Zhejiang Medical Science Institute (Grade II, Certificated No. SCXK2003-0001, weighing 300–330 g). All animal experimental procedures used in this study were in accordance to the guide for the care and use of laboratory animals from Chinese Ministry of Health and approved by Zhejiang University Animal Care and Use Committee. All experiments were reported in compliance with the ARRIVE guidelines (Animal Research: Reporting in Vivo Experiments). Animals were group-housed in individual ventilated cages in temperature-controlled animal holding rooms ($21 \pm 1°C$) on a 12-h reverse light–dark cycle. Animals were acclimatized to housing and experimenters for seven days prior to any experimental manipulation, and were maintained on standard rat chow and water provided ad libitum.

Thirty-three rats were separated into four groups, Male PT stroke group ($n = 11$), Female PT stroke group ($n = 11$), Male sham group ($n = 5$), and Female sham group ($n = 6$). A transparent optical window was assembled on the cortex for PT stroke and chronic optical observation. Briefly, rat was anesthetized with chloral hydrate (10%, 4 ml/kg) and fixed in a stereotaxic apparatus (C6V06-001, RWD Life Science ltd, China). A midline incision was made over the skull and a 3.6×1.8 mm^2 craniotomy was prepared over unilateral cortex (with the center at 4.5 mm posterior and 2 mm lateral to the bregma) using a saline-cooled dental drill (STRONG90, RWD Life Science Ltd, China). The dura was carefully removed and the exposed cortex was covered and protected with 2% agarose (w/v, low-melting point, Sigma-Aldrich, St Louis, MO, USA). A 5 mm diameter round coverglass was following gently pushed on the agarose and glued with the skull by methyl methacrylate acrylic resin (Vertex-Dental, Netherlands). To protect the optical window, a plastic tube with a lid was fixed right above the coverglass with dental cement. During the experimental period, the optical window became cloudy in nine rats due to the inflammation (Male rats: three rats in the stroke group and one rat in the sham group; Female rats: three rats in the stroke group and two rats in the sham group). These nine rats were excluded out of each group, with the final number of 24 rats involved in the analysis (Male rats: eight rats in the stroke group and four rats in the sham group; Female rats: eight rats in the stroke group and four rats in the sham group).

Photothrombotic vascular occlusion

After the rats recovered from initial optical window surgery, PT occlusion was administrated in the ischemia group. Rose Bengal (RB) solution (2.5 mg/100 g, 7.5 mg/mL) was intravenous injection through tail vein right before laser irradiation. The occlusion was induced by focal illumination (1 mm diameter focal spot, 30 mW/mm^2) of 532 nm laser (CNI Laser, Changchun, China) for 30 min, which was focused on the distal middle cerebral arteries (dMCA) near the center of the window. During this period, OCTA imaging was performed every 2 min to monitor clot formation in the region of interest. After PT occlusion, the optical window was strictly shielded from light to minimize diffusive RB activation in the following 24 h. Same surgery and laser irradiation procedure was performed in the sham group, with the RB solution replaced by 0.9% saline solution. Both groups accepted OCTA imaging every day in the following two weeks to monitor the vascular and cellular responses.

Data processing

Angiography. At each scanning step y, adjacent B-frames were paired for blood flow extraction. Fourier transform of the raw spectral interference fringe signal $S(k, x, y, t)$ along the wavenumber k direction was performed to generate reflectivity profile $A(z, x, y, t)$ in the depth (z) space. The absolute value of $A(z, x, y, t)$ was used to generate the structural cross section. The cross-sectional angiogram was then created by subtracting the amplitudes of $A(z, x, y, t)$ between paired B-frames

$$OCTA = \left| A(z, x, y, i + 1) - A(z, x, y, i) \right| \qquad (1)$$

To improve flow contrast, a hybrid averaging strategy was employed.[33] The wavelength and angular diversities were achieved by splitting the wavelength spectrum and the full-space B-scan modulation spectrum, respectively.[33,34] Both the wavelength w and angular a splitting number were set as 2 in this study. The time diversity was achieved by repeated scanning as mentioned above. Five repeated B-frames could generate four sub-angiograms in the time dimension. Totally, $2 \times 2 \times 4$ subangiograms were generated and compounded for the resultant angiogram.

Based on the resultant 3D angiogram, the parameters of flow cross-sectional area (FCA) and vessel area density (VAD)[35] were used for quantifying the vascular structure changes. The surface of brain was
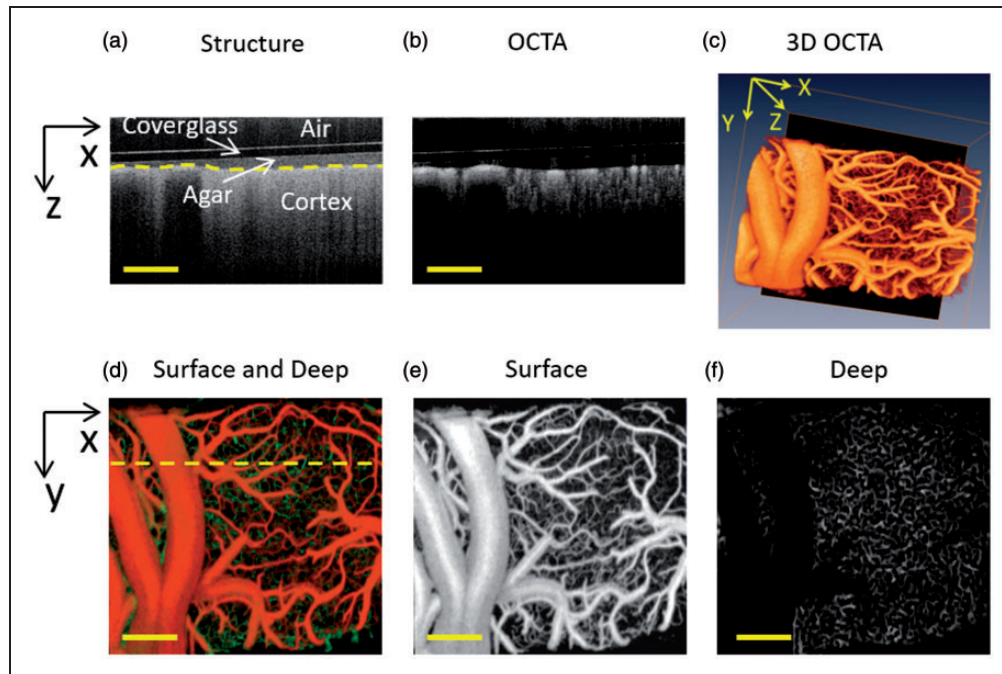
Figure 2. Motion-contrast OCTA-enabled *in vivo* 3D perfusion mapping in rat cortex down to capillary level. (a) OCT structural cross section. Coverglass, agar and cortex were labeled from the top to the bottom. (b) OCTA cross-sectional angiogram. The vessels and capillary bed can be distinguished by different vessel diameters. (c) OCTA 3D perfusion map generated by stacking a series of cross-sectional angiograms. (d) Projection view of the 3D perfusion map in depth direction (surface: orange channel, deep: green channel). (e) and (f) Angiograms at superficial ((e), from surface to depth 100 μm) and deep ((F), depth below 100 μm) layers. Scale bar = 400 μm.

segmented out (referring to Figure 2), and the data above the surface (corresponding to the coverglass and agar) were removed. The 3D angiogram was then separated to the superficial layer (from surface to depth 100 μm) and the deep layer (depth below 100 μm). The angiograms were low-pass filtered to minimize noise, and then binarized with a global threshold. In the binarized superficial layer, the dMCAs were identified manually and quantified with FCA. The average FCA was calculated by counting the number of white pixels and dividing it by pixel number in length direction. Except the dMCAs, the residual vessels in the superficial layer were treated as pial microvasculature. The binarized deep layer was considered as the cortical capillary bed. Both the pial microvasculature and cortical capillary bed were quantified with VAD by calculating the number ratio of white pixels and total pixels.

Scattering coefficient estimation. The light scattering is highly sensitive to morphological changes of cells and organelles, and can be utilized as a potential indicator of brain tissue viability.[25] Due to the optical scattering and absorption of tissue, OCT probe light is attenuated as the beam penetrates deep into tissue. Thus, the OCT depth profile reveals the attenuation coefficient of brain tissue. Assuming the attenuation is mainly contributed by tissue scattering at the 1325 nm wavelength band, local scattering coefficient can be estimated according to the following expression[36,37]

$$\mu_s[i] \approx \frac{I[i]}{2\Delta \sum_{i+1}^{\infty} I[i]} \qquad (2)$$

where $\mu_s[i]$ and $I[i]$ refer to the scattering coefficient and signal intensity for the ith pixel of the OCT image, respectively, and is the pixel size. Thus, a depth-resolved mapping of cellular scattering coefficient can be achieved.

In this study, data processing and analysis were performed with *Matlab* software, and 3D perfusion map were rendered with Amira (ZIB, Indeed-Visual Concepts GmbH, Germany). All the results are expressed as mean ± standard error of the mean.

Results

OCTA-enabled capillary level 3D blood perfusion mapping of rat cortex

Motion-contrast OCTA enabled *in vivo* 3D perfusion mapping of rat cortex down to capillary level. As shown in Figure 2(a), the coverglass, agarose and

cortex were observed clearly in conventional OCT structural cross section. The OCTA cross-sectional angiograms were then generated by analyzing the temporal dynamics of OCT scattering signals (Figure 2(b)). A 3D perfusion mapping (Figure 2(c)) was further achieved by stacking series of sequential cross-sectional angiograms. Figure 2(d) showed the projection view of the 3D perfusion map, which could further be separated into two parts: the superficial slab in orange channel (from surface to 100 µm, Figure 2(e)) and the deep slab in green channel (depth below 100 µm, Figure 2(f)). As we can see, most of the major vessel network was concentrated in the superficial layer with diving arterioles and ascending venules, while there were abundant capillaries inside the deep layer. Therefore, with precise single vessel resolution and depth information, the OCTA imaging could provide a powerful technical means to monitor 3D dynamic changes of vascular structure inside the brain cortex.

OCTA-enabled frequent monitoring of acute PT occlusion progression

The fast imaging speed and large imaging scale make OCTA a perfect tool to monitor the progress of vascular occlusion during acute PT occlusion. Figure 3(a) and (b) shows the dynamic blood flow change of the ischemic region during PT occlusion progress in one male rat. Along with the laser irradiation, the targeted dMCA vessel narrowed with the formation of thrombus on the vessel wall and was blocked completely after 30-min irradiation. At the same time, the capillary perfusion in the deep cortex layer also gradually disappeared. The boundary of the core ischemia area roughly matched with the laser irradiation area (Figure 3(a), green circle) and the perfusion level outside the core area was almost uninfluenced (Figure 3(c)). As shown in Figure 3(b), the occlusion progress could also be observed in the depth z
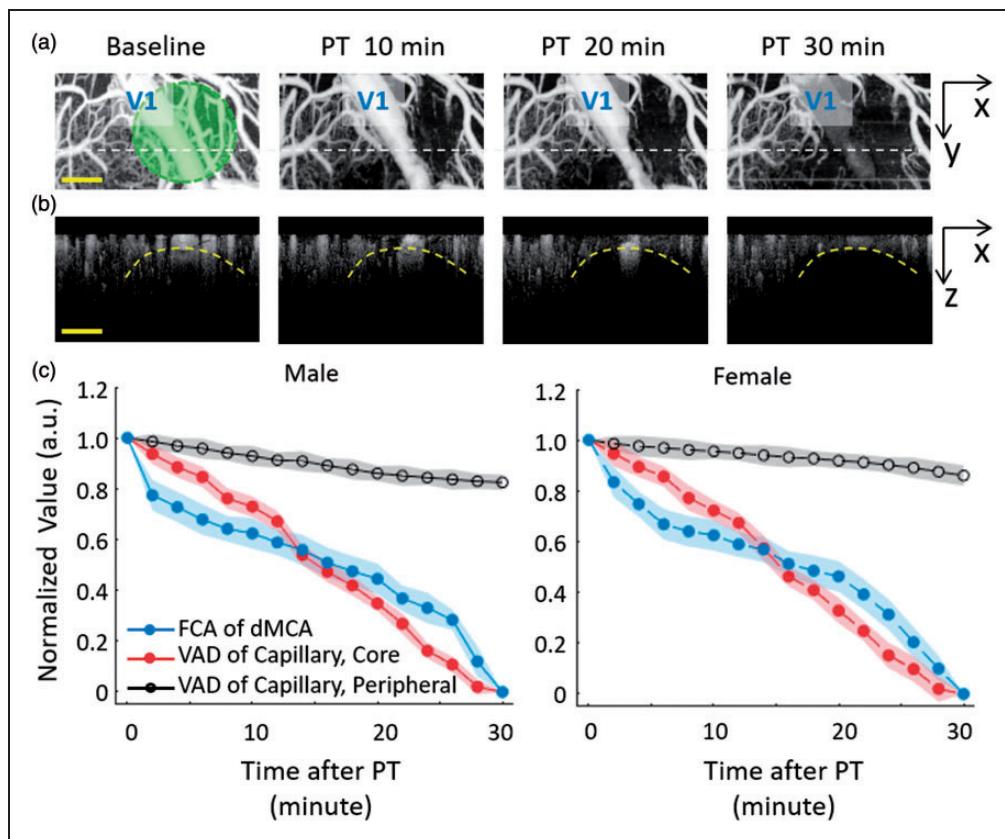

Figure 3. Acute PT occlusion progression with OCTA imaging. (a) The projection views of blood flow perfusion mapping of pre-PT (Baseline condition) and 10, 20, 30 minutes after PT in one male rat. The green circle indicated the laser irradiation region. The corresponding OCTA cross-sections of white dot lines were presented in (b). (c) Relative changes of blood flow in different areas during the PT occlusion formation, including the flow cross-sectional area (FCA) of the distal middle cerebral arteries (dMCA, blue line) and the vessel area density (VAD) of the capillary in the core ischemia region (red line) and the peripheral region (black line). Value was normalized with baseline and presented as Mean ± SD (Male PT Stroke group: $n = 8$; Female PT Stroke group: $n = 8$). Scale bar = 400 µm.
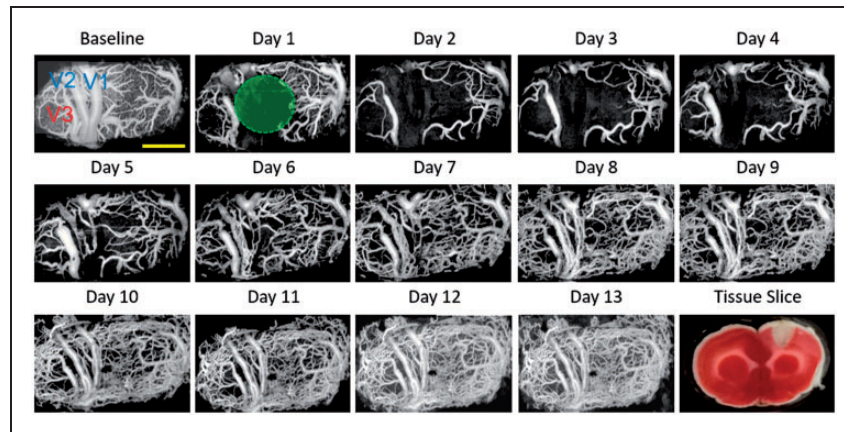
Figure 4. Longitudinal monitoring of chronic post-PT vascular response in the male rat. Chronic monitoring was performed over 13 days. Baseline means the projection view before PT and day 1 means the day of PT administration. The green circle indicates the region of the 30-min laser irradiation. A representative tissue slice at day 1 was presented in the lower right corner. Scale bar = 1 mm.

direction. In the PT occlusion progression, there was no obvious difference between the male and female rats (Figure 3(c)). Since the focus of laser irradiation was adjusted to 500 μm beneath the cortex surface in our PT experiment, the ischemic region was thus spreading from the deep irradiation focus up to the surface area (indicated by the dashed curve in Figure 3(b)). Therefore, with the guidance of 3D OCTA imaging, both the size and spatial location of ischemic lesion can be well controlled with accurate and fast feedback of ischemia degree in acute PT stroke model.

OCTA-enabled longitudinal monitoring of chronic post-PT vascular response

Combined with the chronic optical window on the rat skull, OCTA was suitable for longitudinal monitor of post occlusion blood perfusion. Figure 4 presents typical blood perfusion images in a 3.6×1.8 mm^2 field of view over the chronic post-stroke time course in a male rat. In the baseline image before PT occlusion, the dMCAs, pial microvessels, and the cortical capillary bed could be visualized clearly. Focal ischemic region was then generated after 30-min laser irradiation, where all of the blood flow signal disappeared and no recovery could be recorded at day 1 (1 h after PT formation). In the following three days, the focal ischemic region spread significantly with obvious disappearance of the capillary network outside the irradiation core. Unlike the disappeared small capillaries in the peripheral area, the large size vessels in the peripheral area retained their structure with enlarged diameter (marked as V3, Figure 4). The enlargement of these vessels might be due to the compensation of the impaired vascular supplement in the damaged cortex. The recovery of the blood flow began around day 5, which started with the tiny flow reappearing around the

focal ischemic region. Massive newly appeared blood flows could then be observed both in the ischemic core and peripheral area.

Recanalization of post-PT distal MCA. The capability of single vessel resolution in 3D space facilitates the observation of *in situ* recanalization of dMCA with chronic OCTA imaging. In a typical example of male rats (as shown in Figures 4 and 5(a) and (b)), three large dMCA vessels were identified as the big vessel group, with two of them completely blocked after PT (indicated as V1 and V2 in Figures 4 and 5). PT induced a sharply decreased FCA in the targeted dMCAs and a total occlusion in the following two days (see Figure 5(a) and (b)). Four days after PT occlusion, several fine blood flows appeared right inside the original blocked vessels. These fine blood flows gradually merged together in the following days. For comparison, one example of the female rats is shown in Figure 5(c) and (d). The blocked dMCA in female rat (see the blue dot arrow) presented a similar but faster recovery than the male rat. By comparing the spatial locations of the reappeared blood flow with original vessel, we believe that the recovery of the blocked large dMCA was due to spontaneous thrombolysis and recanalization but not revascularization.

Figure 5(e) demonstrated quantitative analysis of dynamic blood flow changes of large dMCA vessels of all the male and female rats. In male rats, the average FCA of blocked dMCAs quickly decreased to $4 \pm 4\%$ of baseline (mean $\pm$ SD, $n = 8$) after PT damage and slowly recovered to $69 \pm 6\%$ (mean $\pm$ SD, $n = 8$) of baseline at the end point. The lack of the blood flow was compensated by up-regulated diameter of the peripheral unblocked dMCA vessel. Around the last five days, the enlargement of the unblocked dMCAs gradually disappeared and the average FCA returned back
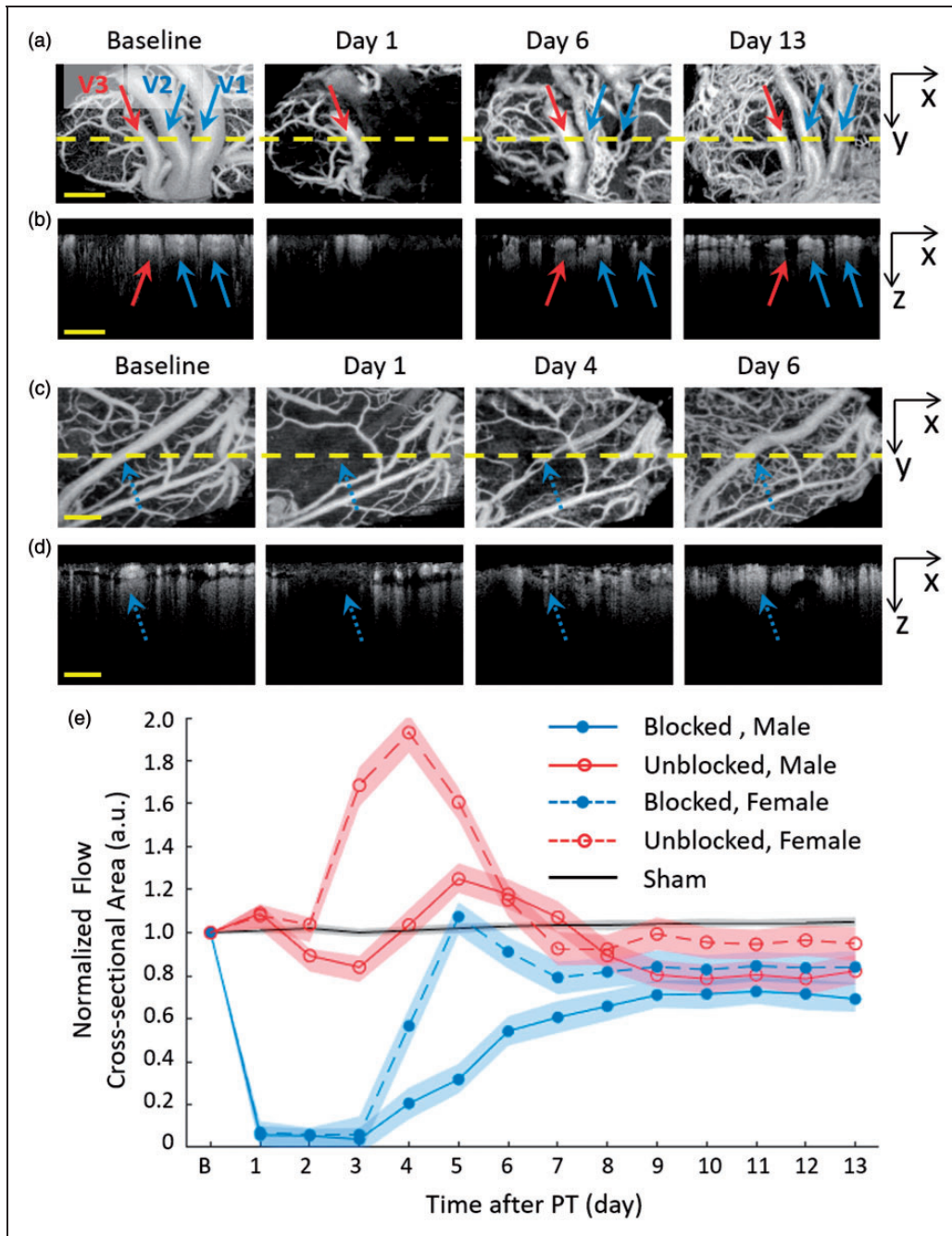
Figure 5. Dynamic blood flow observation of dMCA after PT occlusion. Male: (a) Two of the dMCAs were completely blocked after PT (indicated with blue arrows) in the irradiation core and one vessel in the peripheral area (the red arrow) was less infracted. (b) The cross sections of blood flow imaging of yellow dot line in (a). The recovery blood flow of dMCA (blue arrows) after PT was in the original position and depth as Baseline. Female: (c) The dMCAs was completely blocked after PT (indicated with the blue dot arrows) in the irradiation core. (d) The cross sections of blood flow imaging of yellow dot line in (c). (e) Average flow cross-sectional area (FCA) changes of blocked dMCA in the core ischemia region and the unblocked in the peripheral area of the male and female rats. dMCA: distal middle cerebral arteries.

to around $82 \pm 6\%$ (mean $\pm$ SD, $n = 5$) of the baseline level before PT, indicating partial recovery of vascular network and blood flow in the damaged cortical region. The similar recovery trend was observed in the female

rats, but the enlargement performance of the peripheral unblocked vessels was stronger at day 4 ($193\% \pm 6\%$, mean $\pm$ SD, $n = 5$) and the final recovery degree was higher both in the blocked vessels ($84 \pm 7\%$,
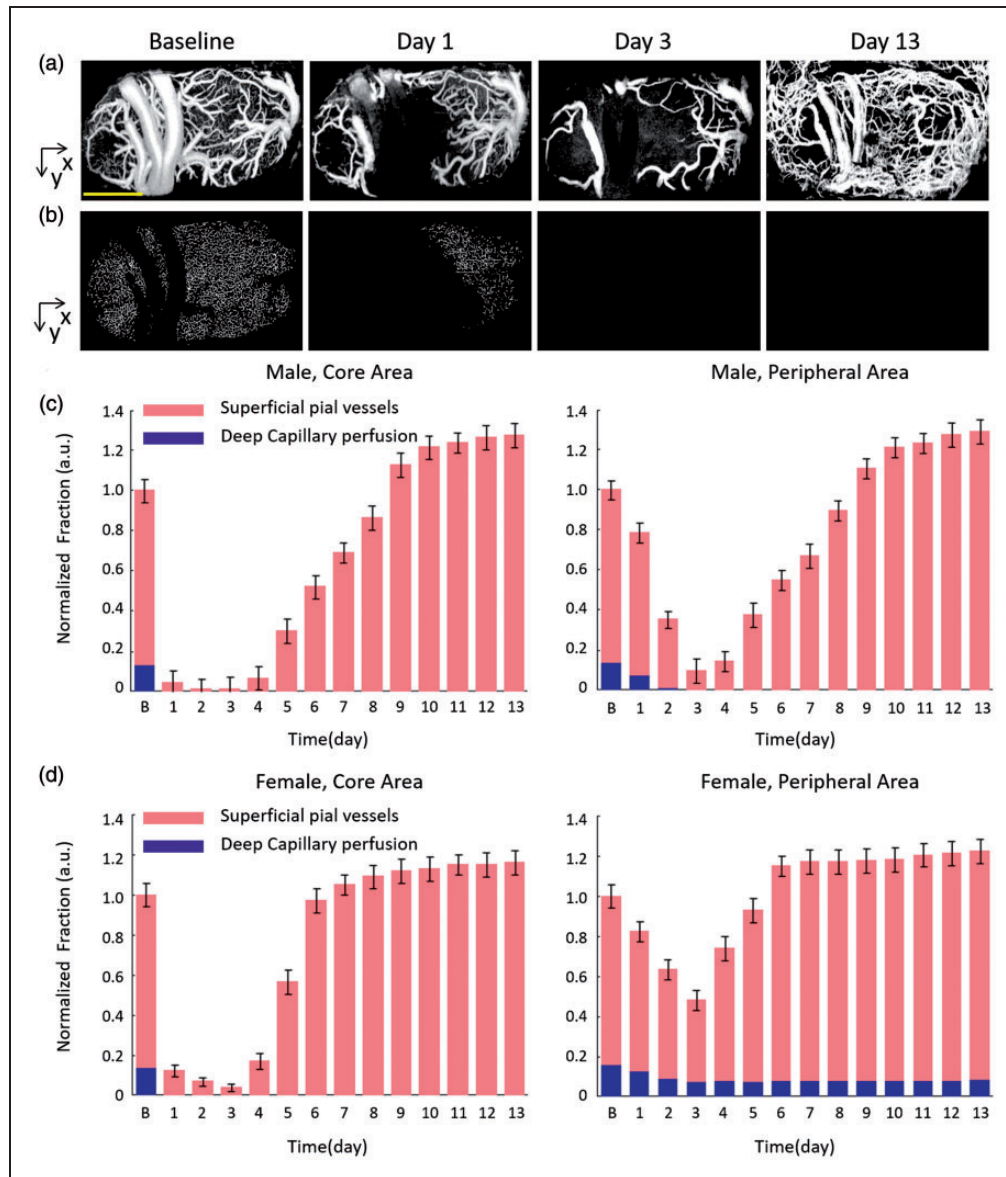
Figure 6. Spontaneous responses of pial microvessels and capillaries network after PT occlusion. The original OCTA perfusion images were segmented into two layers: the superficial layer including pial microvessels ((a), from surface to depth 100 μm) and the deep layer including capillaries ((b), depth below 100 μm). Scale bar = 1 mm. Relative changes of vessel area density (VAD) of the superficial pial microvessels and the deep capillaries network in the irradiation core and the peripheral region of the male rats (c) and the female rats (d).

mean ± SD, $n = 8$) and the peripheral unblocked vessels (95 ± 8%, mean ± SD, $n = 6$).

The diverse responses of pial microvasculature and cortical capillary network after PT occlusion. Different from the thrombolysis and recanalization of large dMCAs, the pial microvessels and cortical capillaries showed various blood flow dynamic changes in chronic recovery period. As mentioned above, the pial microvessels were mainly distributed in the superficial layer and the cortical capillaries were mostly in the deep layer.

In the ischemic core area of male rats, the blood flow of pial microvessels had a rapid drop in the beginning of PT occlusion. The VAD value of pial microvessels constantly decreased to the minimum 3 ± 2% of Baseline at Day 3 (see Figure 6(a) and (c)). After that time point, the occlusion progression reversed with the appearance of blood reperfusion in the superficial pial layer. At the end of two-week recovery period, the VAD of the superficial pial microvessels reached 147 ± 6% of baseline (106 ± 6% in the sham group). Comparatively, in the peripheral area of male rats,

the pial microvessels presented a slower drop in the first three days ($11 \pm 3\%$ of baseline at day 3) and then presented an apparent recovery in the following days ($150 \pm 6\%$ of baseline at Day 13). The pial microvessels of the female group presented a similar time course change, while the female rats took a shorter period of recovery than the male group.

Different from the significant blood flow recovery in the superficial layer, the blood supply in the deep layer presented a permanent damage in the chronic recovery period. In the male group, the cortical capillaries of the core area almost totally disappeared right after the laser irradiation at day 1, while the capillary blood flow in the peripheral area gradually disappeared within the first three days (see Figure 6(b) and (c)). The missing capillary network did not reappear till the end point, which indicates irreversible cortical damage due to the lack of blood supply after PT. The female group presented a similar response of cortical capillary to the male group, except the residual capillaries in the peripheral area. The VAD of the capillaries of the peripheral area in the female group decreased from $82 \pm 6\%$ of baseline at day 1 to $47 \pm 6\%$ at day 3 and remained at this level in the following days (see Figure 6(d)), which might indicate that the female rats had less tissue damage in the peripheral area.

OCT light scattering signal offered a potential indicator of cellular damage

The dynamic changes of scattering coefficient (μ_s) before and after PT might offer an approach to estimate cellular pathophysiological status. To exclude the impact of large vessels and pial microvessels in the superficial layer, the deep cortex layer in the male rat was selected as regions of interest in the following study (indicated with yellow dashed boxes in Figure 7(a) to (c)). As shown in Figure 7(a), the normal brain cortex presented strong backscattering signal intensity before laser irradiation. PT occlusion immediately weakens the backscattering signal in the ischemic core (yellow arrow, Figure 7(a), day 1), while the peripheral region was almost unaffected (Figure 7(a), day 1). The lower backscattering signal region gradually expanded in the following days along with the loss of blood flow (Figure 7(a), day 3). No obvious recovery of the backscattering signal intensity was observed in the subsequent monitoring course. The scattering coefficient imaging of each time point was then calculated as shown in Figure 7(b). Low scattering coefficient value corresponded to weak attenuation of healthy brain tissue and enabled a deep penetration depth as shown in the cortical cross section (Figure 7(b), baseline). Conversely, higher scattering coefficient value corresponded to strong attenuation of infracted brain tissue, which could be observed in the ischemic core right after PT occlusion and the peripheral area in the recovery period. The cross-sectional imaging revealed that the tissue scattering changes had a high spatiotemporal correlation with the perfusion changes (Figure 7(c)). Figure 7(d) reported representative projection views of 3D scattering coefficient mapping. By setting an appropriate scattering threshold, scattering-determined boundaries of the ischemia core and
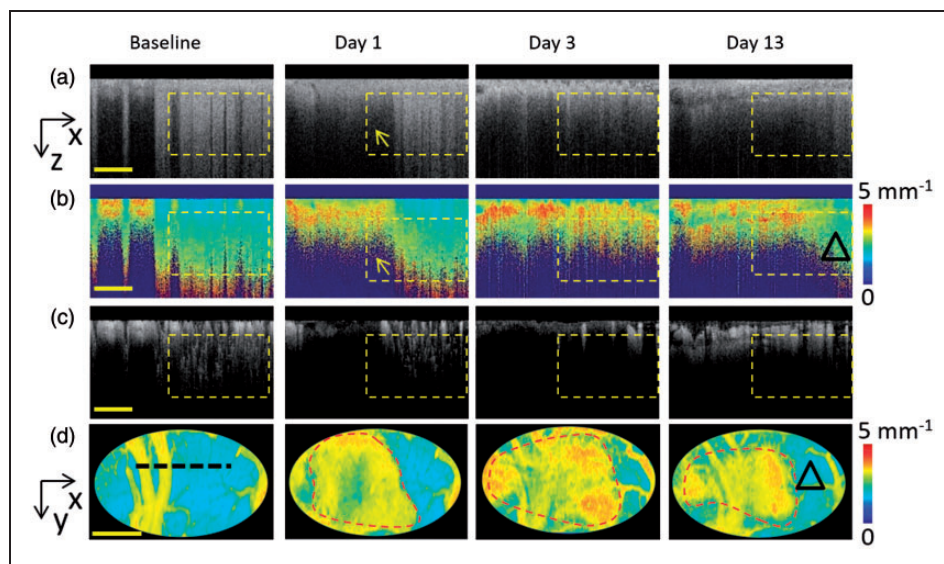

Figure 7. Dynamic changes of cellular scattering. (a) From the left to the right, the original OCT structural cross sections of baseline, and at day 1, day 3 and day 13. (b) Scattering coefficient cross sections corresponding to the structural images in (a). (c) OCTA cross-sectional angiograms corresponding to the structural images in (a). Scale bar = 400 μm. (d) The projection pseudo-color images of 3D scattering coefficient corresponding to the region of Figure 4 of baseline, day 1, day 3 and day 13. The lesion boundary is marked with the red dot line after PT. Scale bar = 1 mm.

peripheral areas can be generated (red dash line in Figure 7(d)). Roughly, the scattering-determined boundaries agreed well with the blood perfusion changes in Figure 6, which further confirmed the spatiotemporal correlation between tissue scattering and blood perfusion. It should be noted that a certain reverse of scattering coefficient was observed in the peripheral region at day 13, as marked by a black triangle in Figure 7(d). The similar correlationship was also observed in female rats.

Discussion and conclusion

In this study, parallel analyses of spatiotemporal dynamics of both blood perfusion and cellular scattering were performed with OCT in chronic rat PT stroke model in a label-free and depth-resolved manner. The 3D mapping of blood perfusion and cellular scattering were achieved by analyzing the temporal dynamics and the depth attenuation of the backscattered light, respectively. Compared with the depth-integrated two-dimensional blood flow mapping in LSCI, OCTA offers a 3D visualization of the cortical perfusion down to capillary level, which enables the observation of the different vascular responses. On the other hand, in contrast to dye-based 2P microscopy, the label-free, motion-contrast OCTA allows vascular examinations as frequently as required during the entire progression.

OCTA allows a fast and frequent vascular examination over a several millimeter field-of-view during the acute PT occlusion progression, suggesting an effective feedback and precise control of ischemia content during laser irradiation. In the current study, real-time monitoring of the acute PT occlusion procedure was performed by 2D cross sections. During this period, 3D datasets were acquired every 2 min. The data processing and image rendering of the 3D perfusion map were performed off line due to the limitation of graphics processing speed of our computer. MHz ultrafast OCT imaging and GPU-based real-time processing and displaying can be implemented for real-time 3D vascular examination in the near future, which could improve the control of cortical ischemia damage and increase the stability and repeatability of the PT model.

During the longitudinal observation in the chronic stroke model, vessels of different types presented different spatial and temporal dynamics. With the direct visualization of single vessel in OCTA, the cross-sectional area and depth distribution of blood flow signal can thus be assessed accurately along with the chronic recovery period. As shown in our experiment, the first three days after PT occlusion can be identified as acute phase of vessel thrombosis, with all dMCAs, pial microvessels and capillaries disappearing right after laser irradiation. The blood flow of peripheral area gradually lost and the ischemia area expanded most at day 3. After that time point, the blood flow began to recover from the peripheral area to the ischemia core. In the male rats, the recanalization of major dMCA vessels occurred about one week after laser irradiation, while the pial microvasculature presented a well recovery of blood perfusion. Different from dMCAs and pial microvessels, no capillary recovery was observed both in the core and peripheral areas till the end of observation in the male rats. However, the recanalization of the blocked dMCA vessels in the female rats occurred 1–2 days earlier than the male rats and the female rats had a certain of residual capillary perfusion in the peripheral areas. The observation is consistent with the early research about the gender difference in ischemic stroke and trauma animal models. Early researches by Alkayed et al. showed that female rats maintain higher CBF and sustain smaller infarct size after middle cerebral artery occlusion (MCAO) compared with male rats, and the difference in blood flow and relative protection from stroke in female rats was lost after ovariectomy. Female rats may be affected by higher estrogen concentration and lower epoxide hydrolase concentration, which was demonstrated to cause the gender-specific vascular response to cerebral ischemia after trauma.[38–40]

The spatial and temporal dynamics of blood perfusion may be related to the PT occlusion model used in this study. PT occlusion model is widely adopted in previous rodent stroke researches, with fine controllable location and degree of focal ischemia. PT stroke model can mimic the small stroke with small injury and focal ischemia in the cortical surface. Using chronic cranial window, surgeries on the skull and dura altered intra-cranial pressure and might induce inflammation, which led to a success rate of 73% for repeated daily imaging in this experiment. However, a limitation of this occlusion model is early vasogenic edema and blood–brain barrier breakdown throughout the illuminated region, resulting in a larger ischemic core and smaller penumbra area than other stroke models which targeted only one major vessel such as MCA.[41] Therefore, PT model may cause severe cell damage inside the laser illuminate area and activate a series of following cellular reactions, which may change the physiochemical characteristics of the brain tissue and influence the recovery of capillary inside the damaged cortex. Combined with well-designed PT stroke model and the chronic optical window technology, OCTA imaging should be an appropriate tool for chronic blood dynamic observation and could be widely adopted in various applications in the future, such as neurovascular coupling research, neural system drug screen, neural modulation of neural diseases and rehabilitation from brain injury.[42]

As a potential indicator of brain tissue viability, the cellular scattering coefficient was also measured with OCT. The PT-induced ischemic region presented a weakened OCT intensity signal and an increased scattering coefficient, which was used to indicate the tissue damage in the transient MACO stroke model.[25,26] Vivek et al. demonstrated that intrinsic scattering markers can act as non-invasive indicators of cell status and viability.[43] The early increase of the scattering coefficient can be ascribed to the tissue damage after ischemia, which is in agreement with Ruikang Wang et al.[25,26] And the later reverse of the scattering coefficient in the peripheral area is most likely due to the changes of the cellular morphology and type. Li et al.[44] observed the proliferation from day 1 to day 14 in ischemic core and from day 1 to day 8 in the peripheral area (200–400 μm far away from the edge of the ischemic core). And our results were spatiotemporally consistent with the histological changes reported by Li et al.[44] As a potential indicator of brain tissue viability, scattering coefficient can be evaluated in parallel with the blood perfusion within the tissue bed in OCTA. The comparative analysis revealed a spatiotemporal correlation between the cellular damage and capillary perfusion. Further study is required to comprehensively understand the physiological mechanism of the cellular scattering changes.

In summary, combined with well-designed PT stroke model and chronic optical window, OCT imaging offers a unique approach to improving the understanding of stroke and evaluating the treatment. The functional recovery behavior of the blood vessels and neuron following ischemic stroke was a key role in the therapy methods against brain damage. Further well-designed studies are required to systematically investigate the complex mechanisms of ischemia and tissue injury, which would be helpful to the clinical treatment for ischemic stroke and other diseases.

Funding

Declaration of conflicting interests

The author(s) declared no potential conflicts of interest with respect to the research, authorship, and/or publication of this article.

Authors' contribution

PL, KX and KL conceived and designed the study; PL and SY designed and built the system; KX, KL, HD and HG prepared the animals; PL, KX, KL and SY analyzed the data; PL, KX, KL, SY, XZ and ZD wrote the manuscript; SY and KL contributed equally to this work.

References

1. Brott TG and Bogousslavsky J. Treatment of acute ischemic stroke. *N Engl J Med* 2000; 343: 710–722.
2. Mukherjee D and Patil CG. Epidemiology and the Global Burden of Stroke. *World Neurosurg* 2011; 76: S85–S90.
3. Molina CA. Reperfusion therapies for acute ischemic stroke current pharmacological and mechanical approaches. *Stroke* 2011; 42: S16–S19.
4. Murphy TH and Corbett D. Plasticity during stroke recovery: from synapse to behaviour. *Nat Rev Neurosci* 2009; 10: 861–872.
5. Font MA, Arboix A and Krupinski J. Angiogenesis, neurogenesis and neuroplasticity in ischemic stroke. *Curr Cardiol Rev* 2010; 6: 238–244.
6. Schoknecht K, Prager O, Vazana U, et al. Monitoring stroke progression: in vivo imaging of cortical perfusion, blood–brain barrier permeability and cellular damage in the rat photothrombosis model. *J Cereb Blood Flow Metab* 2014; 34: 1791–1801.
7. Denk W, Strickler JH and Webb WW. Two-photon laser scanning fluorescence microscopy. *Science* 1990; 248: 73–76.
8. Kleinfeld D, Mitra PP, Helmchen F, et al. Fluctuations and stimulus-induced changes in blood flow observed in individual capillaries in layers 2 through 4 of rat neocortex. *Proc Natl Acad Sci U S A* 1998; 95: 15741–15746.
9. Schrandt CJ, Kazmi SM, Jones TA, et al. Chronic monitoring of vascular progression after ischemic stroke using multiexposure speckle imaging and two-photon fluorescence microscopy. *J Cereb Blood Flow Metab* 2015; 35: 933–942.
10. Dunn AK, Bolay T, Moskowitz MA, et al. Dynamic imaging of cerebral blood flow using laser speckle. *J Cereb Blood Flow Metab* 2001; 21: 195–201.
11. Yin B, Kuranov RV, McElroy AB, et al. Dual-wavelength photothermal optical coherence tomography for imaging microvasculature blood oxygen saturation. *J Biomed Optics* 2013; 18: 56005.
12. Huang D, Swanson EA, Lin CP, et al. Optical coherence tomography. *Science* 1991; 254: 1178–1181.
13. Wang RK, Jacques SL, Ma Z, et al. Three dimensional optical angiography. *Opt Express* 2007; 15: 4083–4097.
14. Chen CL and Wang RK. Optical coherence tomography based angiography [Invited]. *Biomed Optics Express* 2017; 8: 1056–1082.
15. Makita S, Hong Y, Yamanari M, et al. Optical coherence angiography. *Opt Express* 2006; 14: 7821–7840.
16. Fingler J, Schwartz D, Yang C, et al. Mobility and transverse flow visualization using phase variance contrast with spectral domain optical coherence tomography. *Opt Express* 2007; 15: 12636–12653.

17. Mariampillai A, Standish BA, Moriyama EH, et al. Speckle variance detection of microvasculature using swept-source optical coherence tomography. *Optics Lett* 2008; 33: 1530–1532.

18. Cheng Y, Guo L, Pan C, et al. Statistical analysis of motion contrast in optical coherence tomography angiography. *J Biomed Optics* 2015; 20: 116004.

19. Enfield J, Jonathan E and Leahy M. In vivo imaging of the microcirculation of the volar forearm using correlation mapping optical coherence tomography (cmOCT). *Biomed Optics Express* 2011; 2: 1184–1193.

20. Jia Y, Tan O, Tokayer J, et al. Split-spectrum amplitude-decorrelation angiography with optical coherence tomography. *Opt Express* 2012; 20: 4710–4725.

21. Jia Y, Alkayed N and Wang RK. The potential of optical micro-angiography to monitor cerebral blood perfusion and vascular plasticity following traumatic brain injury in mice in vivo. *J Biomed Optics* 2009; 14: 040505.

22. Mourant JR, Freyer JP, Hielscher AH, et al. Mechanisms of light scattering from biological cells relevant to non-invasive optical-tissue diagnostics. *Appl Optics* 1998; 37: 3586–3593.

23. Vakoc BJ, Lanning RM, Tyrrell JA, et al. Three-dimensional microscopy of the tumor microenvironment in vivo using optical frequency domain imaging. *Nat Med* 2009; 15: 1219–U151.

24. Baran U, Zhu W, Choi WJ, et al. Automated segmentation and enhancement of optical coherence tomography-acquired images of rodent brain. *J Neurosci Meth* 2016; 270: 132–137.

25. Kawauchi S, Sato S, Uozumi Y, et al. Light-scattering signal may indicate critical time zone to rescue brain tissue after hypoxia. *J Biomed Optics* 2011; 16: 027002–027008.

26. Srinivasan VJ, Mandeville ET, Can A, et al. Multiparametric, longitudinal optical coherence tomography imaging reveals acute injury and chronic recovery in experimental ischemic stroke. *PLoS One* 2013; 8: e71478.

27. Baran U, Li Y and Wang RK. In vivo tissue injury mapping using optical coherence tomography based methods. *Appl Optics* 2015; 54: 6448–6453.

28. Llovera G, Roth S, Plesnila N, et al. Modeling stroke in mice: permanent coagulation of the distal middle cerebral artery. *JoVE* 2014; 89: e51729.

29. Labatgest V and Tomasi S. Photothrombotic ischemia: a minimally invasive and reproducible photochemical cortical lesion model for mouse stroke studies. *JoVE* 2013; 76: e50370.

30. Schaffer CB, Friedman B, Nishimura N, et al. Two-photon imaging of cortical surface microvessels reveals a robust redistribution in blood flow after vascular occlusion. *Plos Biol* 2006; 4: e22.

31. Liu Q, Li Y, Lu H, et al. Real-time high resolution laser speckle imaging of cerebral vascular changes in a rodent photothrombosis model. *Biomed Optics Express* 2014; 5: 1483–1493.

32. Vakoc BJ, Tearney GJ and Bouma BE. Statistical properties of phase-decorrelation in phase-resolved Doppler optical coherence tomography. *Transact IEEE: Med Imag* 2009; 28: 814–821.

33. Li P, Cheng Y, Li P, et al. Hybrid averaging offers high-flow contrast by cost apportionment among imaging time, axial, and lateral resolution in optical coherence tomography angiography. *Optics Lett* 2016; 41: 3944–3947.

34. Li P, Cheng Y, Zhou L, et al. Single-shot angular compounded optical coherence tomography angiography by splitting full-space B-scan modulation spectrum for flow contrast enhancement. *Optics Lett* 2016; 41: 1058–1061.

35. Reif R, Qin J, An L, et al. Quantifying optical microangiography images obtained from a spectral domain optical coherence tomography system. *Int J Biomed Imag* 2012; 2012: 509783.

36. Vermeer KA, Mo J, Weda JJ, et al. Depth-resolved model-based reconstruction of attenuation coefficients in optical coherence tomography. *Biomed Optics Express* 2013; 5: 322–337.

37. Guo L, Shi R, Zhang C, et al. Optical coherence tomography angiography offers comprehensive evaluation of skin optical clearing in vivo by quantifying optical properties and blood flow imaging simultaneously. *J Biomed Optics* 2016; 21: 081202.

38. Zhang W, Iliff JJ, Campbell CJ, et al. Role of soluble epoxide hydrolase in the sex-specific vascular response to cerebral ischemia. *J Cereb Blood Flow Metab* 2009; 29: 1475–1481.

39. Jia Y, Grafe MR, Gruber A, et al. In vivo optical imaging of revascularization after brain trauma in mice. *Microvasc Res* 2011; 81: 73–80.

40. Alkayed NJ, Harukuni I, Kimes AS, et al. Gender-linked brain injury in experimental stroke. *Stroke* 1998; 29: 159–166.

41. Howells DW, Porritt MJ, Rewell SSJ, et al. Different strokes for different folks: the rich diversity of animal models of focal cerebral ischemia. *J Cereb Blood Flow Metab* 2010; 30: 1412–1431.

42. Phillips AA, Chan FH, Zheng MMZ, et al. Neurovascular coupling in humans: Physiology, methodological advances and clinical implications. *J Cereb Blood Flow Metab* 2016; 36: 647–664.

43. Srinivasan VJ, Radhakrishnan H, Jiang JY, et al. Optical coherence microscopy for deep tissue imaging of the cerebral cortex with intrinsic contrast. *Optics Express* 2012; 20: 2220–2239.

44. Li H, Zhang N, Lin H, et al. Histological, cellular and behavioral assessments of stroke outcomes after photothrombosis-induced ischemia in adult mice. *BMC Neurosci* 2014; 15: 58.

45. Rodriguez CL, Szu JI, Eberle MM, et al. Decreased light attenuation in cerebral cortex during cerebral edema detected using optical coherence tomography. *Neurophotonics* 2014; 1: 025004.